Selective Tumor Targeting by the Hypoxia-Activated Prodrug AQ4N Blocks Tumor Growth and Metastasis in Preclinical Models of Pancreatic Cancer

Alshad S. Lalani,[1] Susan E. Alters,[1] Alvin Wong,[1] Mark R. Albertella,[2] Jeffrey L. Cleland,[1] and William David Henner[1]

Abstract

Purpose: The antitumor activities and pharmacokinetics of the hypoxia-activated cytotoxin AQ4N and its metabolites were assessed in several preclinical models of pancreatic cancers.

Experimental Design: The cytotoxic effects of AQ4N prodrug and its bioreduced form, AQ4, were tested against multiple human tumor cell lines using 3-(4,5-dimethylthiazol-2-yl)-2,5-diphenyltetrazolium bromide assays. Nude mice bearing s.c. or orthotopically implanted human BxPC-3 or Panc-1 tumor cells were treated with AQ4N. Tumor growth inhibition, time to progression/end point, and liver metastasis were evaluated in treatment versus control groups. Plasma and tumor levels of AQ4N and its metabolites were quantitated by liquid chromatography-tandem mass spectrometry.

Results: In contrast to AQ4N, the bioreduced AQ4 metabolite displayed potent cytotoxicity in many human tumor lines, including those derived from human pancreatic adenocarcinomas. Single-agent administration of AQ4N significantly delayed tumor growth, progression, and survival in a manner comparable with gemcitabine in multiple pancreatic tumor models *in vivo*. Survival increases were accompanied by a reduction in incidence and spread of liver metastasis. Quantitation of AQ4N and its metabolites in tumor-bearing mice showed that the prodrug is rapidly cleared from the circulation by 24 h and neither of the bioreduced metabolites was detected in plasma. In contrast, AQ4N readily penetrated BxPC-3 tumors and the cytotoxic AQ4 metabolite rapidly accumulated in tumor tissues at high levels in a dose-dependent fashion.

Conclusion: AQ4N undergoes rapid and selective conversion into the potent antineoplastic metabolite AQ4 in tumors *in vivo* and provides proof of principle for the use of hypoxia-activated prodrugs in the treatment against pancreatic cancers.

Generation of compounds that selectively eliminate tumor cells with minimal toxicity to normal tissues is a key goal in the development of safe and effective antineoplastic agents. One strategy to achieve tumor selectivity is to exploit the low levels of oxygenation, or hypoxia, which is a common characteristic of many solid tumors (1–4). Pancreatic adenocarcinoma, currently the fourth leading cause of cancer deaths in the United States (5), is characterized by regions of hypovascularity as shown by imaging diagnostics (6–9). Direct intratumoral oxygen measurements using polagraphic electrode probes have also verified that pancreatic tumors are significantly more hypoxic than adjacent normal tissues (10). Cellular hypoxia within the tumor microenvironment triggers changes in the transcriptional regulation of many genes involved in cellular metabolism, angiogenesis, and metastasis, further propagating tumor growth and spread (1, 11–16). For example, tumor hypoxia has been shown to influence metastatic disease progression of pancreatic cancers in orthotopic rodent models (17). In humans, the extent of tumor hypoxia seems to inversely correlate with patient prognosis and is often associated with resistance to conventional treatment modalities (12, 14, 18, 19). Thus, tumor-associated hypoxia presents a unique opportunity to specifically target regions of the tumor that are refractory to conventional treatments.

Hypoxia-selective cytotoxins are a new class of drugs that are activated into cytotoxic agents under conditions of low oxygen tension as found in central and peripheral regions of solid tumors. One promising agent currently under clinical investigation is the di-*N*-oxide aliphatic amino anthracenedione, AQ4N (banoxantrone; 1,4-bis{[2-(dimethylamino)ethyl]amino}-5,8-hydroxyanthracene-9,10-dione bis-*N*-oxide; refs. 20–22). AQ4N is relatively noncytotoxic until it is metabolically activated in hypoxic tumor cells by two-step enzymatic reduction first to form AQ4M, a short-lived mono-*N*-oxide intermediate, and then to AQ4, a fully bioreduced ditertiary cationic amine (21, 23, 24). Bioactivation of AQ4N to AQ4 occurs strictly in low oxygen environments and involves a

Authors' Affiliations: [1]Novacea, Inc., South San Francisco, California and [2]KuDOS Pharmaceuticals Ltd., Cambridge, United Kingdom

Received 10/3/06; revised 12/18/06; accepted 1/11/07.

The costs of publication of this article were defrayed in part by the payment of page charges. This article must therefore be hereby marked *advertisement* in accordance with 18 U.S.C. Section 1734 solely to indicate this fact.

Requests for reprints: Alshad S. Lalani, Novacea, Inc., 601 Gateway Boulevard, Suite 800, South San Francisco, CA 94080. Phone: 650-228-1882; Fax: 650-228-1087; E-mail: lalani@novacea.com.

doi:10.1158/1078-0432.CCR-06-2427

four-electron reduction process, which seems to be mediated by cytochrome *P*450 (CYP) enzymes, including CYP3A4, CYP1A1, CYP1A2, and CYP2B6 (21, 23, 25–31). Many of these *P*450 isoforms are differentially expressed in a wide spectrum of human tumors and may contribute to the liberation of the cytotoxic AQ4 metabolite within hypoxic regions of tumors (32, 33). Once fully reduced, the highly stable AQ4 metabolite intercalates into DNA with high avidity, where it functions as a potent inhibitor of topoisomerase II, thereby arresting cellular proliferation (23, 24, 34, 35).

Tumor selectivity following AQ4N treatment in experimental human solid tumor models has not been well characterized. Given the extremely low oxygen tension found in pancreatic tumors and the selective bioactivation of AQ4N in hypoxic microenvironments, we hypothesized that AQ4N may have therapeutic utility in this aggressive neoplasm. Therefore, we evaluated the efficacy and tumor-targeting activity of AQ4N *in vivo* using multiple pancreatic xenograft models. *In vitro*, the bioreduced AQ4 metabolite showed potent antiproliferative activity in contrast to the low cytotoxic activity displayed by the AQ4N prodrug against a broad spectrum of human tumor lines. Here, we show that administration of AQ4N as a single agent has significant tumor growth-inhibitory and antimetastatic effects, in addition to prolonging the survival of nude mice bearing s.c. or orthotopically implanted human pancreatic tumors. Moreover, plasma and tumor pharmacokinetics following drug infusion reveal a dose-dependent accumulation of the fully bioreduced AQ4 cytotoxic metabolite in tumor tissues and a rapid clearance of the AQ4N prodrug from the systemic circulation. Thus, AQ4N may represent a novel tumor-targeting cytotoxic prodrug, which warrants further investigation in human clinical studies for the treatment of hypoxic tumors, such as pancreatic adenocarcinomas.

Materials and Methods

IC_{50} determination on a panel of tumor lines. Standard human tumor cell lines were obtained commercially and plated at appropriate cell densities (based on the *in vitro* doubling time of each cell line) in 96-well flat-bottomed microtiter plates and incubated at 37°C for 24 h in 0.1 mL of drug-free RPMI 1640 supplemented with 10% fetal bovine serum. Cells were subsequently exposed to AQ4, AQ4N, or a relevant chemotherapeutic agent (as a positive control, see Table 1) for 24 h under normoxic conditions in a 37°C humidified incubator. AQ4 was dissolved in 0.1% formic acid and then diluted in sterile water. AQ4N was dissolved in PBS, the pH adjusted to 6.8 using 5 N NaOH, and then diluted in RPMI 1640. Control cells were treated with the appropriate vehicle alone. Drug-containing medium was washed out and replaced by drug-free medium, and tumor cells were incubated for an additional 72 h. Cell viability was evaluated using a 3-(4,5-dimethylthiazol-2-yl)-2,5-diphenyltetrazolium bromide assay, and the IC_{50}, defined as the concentration of drug required to block 50% cell viability, was determined using Genesis software (Labsystem, Helsinki, Finland). Each assay point was done in quadruplicate, and the experiment was repeated thrice per cell line.

S.c. Panc-1 xenograft model. Panc-1 tumor fragments ($\sim$1 mm^3) were implanted s.c. into female nude (*nu/nu*) mice (Harlan, Inc., Indianapolis, IN). When the tumors reached $\sim$100 mm^3 in size (25 days following implantation), the animals were pair matched into 10 mice per group and treatment was initiated according to the schedule/doses indicated in the text. AQ4N, formulated in PBS, and gemcitabine (Gemzar, Eli Lilly and Company, Indianapolis, IN), formulated in 0.9% NaCl, were prepared on each day of dosing and delivered by i.v. and i.p. administration, respectively. The dose and

Table 1. Effects of AQ4, AQ4N, and standard agents on cell viability against a panel of human solid tumor lines *in vitro*

Tumor line	Tumor type	AQ4 IC_{50} (μmol/L)	AQ4N IC_{50} (μmol/L)	Standard agent IC_{50} (μmol/L)
BxPC-3	Pancreatic	1.6	NA*	0.060 (gemcitabine)
Panc-1	Pancreatic	0.4	NA*	1.70 (gemcitabine)
Mia PaCa-2	Pancreatic	1.6	NA*	0.020 (gemcitabine)
HT-29	Colon	0.7	101.5	0.087 (SN38)
HCT-116	Colon	3.9	NA*	0.900 (SN38)
LoVo	Colon	0.2	49.9	0.024 (SN38)
LS174T	Colon	0.7	14.4	0.106 (SN38)
MCF-7	Breast	0.3	NA*	0.002 (paclitaxel)
MDA-MB-231	Breast	2.7	NA*	NA (paclitaxel)
A-498	Renal cell	2.5	NA*	NA (paclitaxel)
Caki-1	Renal cell	1.8	NA*	NA (paclitaxel)
A2780	Ovarian	0.05	12.3	0.001 (paclitaxel)
OVCAR-3	Ovarian	2.7	NA*	0.015 (paclitaxel)
A549	NSCLC	0.1	85.4	0.010 (paclitaxel)
H460	NSCLC	1.4	103.0	0.006 (paclitaxel)
PC-3	Prostate	11.2	NA*	0.007 (paclitaxel)
LNCap-FGC	Prostate	0.8	43.0	0.002 (paclitaxel)
FaDu	Pharynx SCC	0.3	64.7	7.01 (paclitaxel)
KB	Oral carcinoma	0.6	13.4	2.00 (paclitaxel)
KB-3	Rad-resistant KB	3.3	NA*	19.10 (paclitaxel)
Hep3B2,1-7	Hepatocellular	0.8	NA*	1.40 (paclitaxel)
A375	Melanoma	3.3	NA*	0.006 (paclitaxel)

NOTE: The mean IC_{50} values were determined from three independent experiments. IC_{50} was determined by a 3-(4,5-dimethylthiazol-2-yl)-2,5-diphenyltetrazolium bromide assay following 24-h drug exposure as described in the text.
Abbreviation: NSCLC, non–small cell lung cancer.
*Nonachievable under the physiologic/normoxic conditions tested.

schedule of gemcitabine were selected based on prior experience with gemcitabine in these *in vivo* models (36). Panc-1 tumors were measured with calipers twice weekly, and tumor volume was calculated using the following formula: tumor volume (mm^3) = [(width)^2 × length] / 2. Animals were monitored for signs of toxicity and weighed daily for the first 5 days of the study and then twice weekly until the study end. As predefined in the protocol, each animal was actively euthanized when its tumor reached the predetermined end point size of 1,200 mm^3 or at the conclusion of the study (day 60), whichever came first. The time to end point was calculated for each mouse as time to end point (days) = [$\log_{10}$(end point volume mm^3) − b] / m, where b is the intercept and m is the slope of the line obtained by linear regression of a log-transformed tumor growth data set. Treatment outcome was determined from tumor growth delay (TGD), which is defined as the increase in median time to end point in a treatment (T) group compared with the control (C) group (TGD = T − C) expressed in days or as a percentage of the median time to end point of the control group %TGD = [(T − C) / C] × 100.

Kaplan-Meier plots were constructed to show the percentage animals remaining in the study as a function of time following treatment. Statistical significance between the treated versus control groups was evaluated by log-rank analysis using Prism GraphPad software (GraphPad, San Diego, CA).

S.c. BxPC-3 xenograft model. Female nude mice (*nu/nu*) were implanted s.c. with fragments of human BxPC-3 pancreatic tumors. When the tumors reached approximately 60 to 80 mm^3 in size, the animals were pair matched into treatment and control groups containing 10 mice per group. Treatment administration of AQ4N (i.v.) or gemcitabine (i.p.) was initiated the day the animals were pair matched (day 1). Tumors were measured by calipers twice weekly and converted to tumor volume by the following formula: tumor volume (mm^3) = [(width)^2 × length] / 2. The experiment was terminated when the vehicle control group tumor size reached an average of ~2,000 mm^3 (~27 days). On termination, the mice were weighed and sacrificed, tumors were excised, and the mean tumor volume per group was calculated. Tumor growth inhibition (TGI), defined as the change in mean tumor volume of the treated groups/the change in mean tumor volume of the control group × 100 (ΔT/ΔC), was calculated for each group. Statistical comparisons were carried out using ANOVA followed by the Dunnett multiple comparisons test. All statistical analyses were done with Prism GraphPad software.

Orthotopic BxPC-3 xenograft model and histologic analysis. Female athymic NMRI mice were injected with 2.5 × 10^6 human BxPC-3 pancreatic cells directly into the pancreas parenchyma. Treatment with AQ4N (i.v.) or gemcitabine (i.p.) was initiated on day 14 after tumor implantation at the dose/schedules indicated in the text. Treatment groups consisted of 12 mice; an extra 5 mice were added to each group for histologic analysis. In the orthotopic BxPC-3 model, mice were monitored twice daily for symptoms of disease and actively euthanized based on the criteria outlined by the Institutional Ethical Committee; the day of sacrifice is considered the day of cancer death. Prolongation of survival, a primary end point in this study, was evaluated using Kaplan-Meier plots, and statistical significance of treatment responses compared with control groups was analyzed by log-rank analysis using Prism GraphPad software. For histologic analysis, mice were sacrificed on day 36 after tumor implantation. Primary tumors and livers, a target organ for metastases formation in this model, were resected and paraffin embedded. Formalin-fixed, paraffin-embedded tissue sections (5 μm thick) were stained with H&E as described previously (37). Five slides were prepared per tissue for each of the mice (n = 5/group), and gross histopathologic analysis was done. To compute the metastasis index, blinded liver sections were analyzed by microscopy by two independent pathologists. The total percentage of space occupied by invasive tumor cells was enumerated and expressed as a percentage of total tissue evaluated. Statistical analysis was computed using the nonparametric Mann-Whitney U test.

Pharmacokinetic studies. Female C-17 severe combined immunodeficient mice (IFFA CREDO, L'Arbresles, France) were irradiated with a γ source (1.8 Gy, Co-60, INRA, Dijon, France) 24 h before s.c. injection with 1 × 10^7 BxPC-3 cells. Animals were dosed when the mean tumor volume reached 266 ± 88 mm^3 (day 53). Mice were randomized into four groups of nine mice. The mice received a single i.v. bolus injection of AQ4N at 20, 60, 120, or 240 mg/kg via the caudal vein. Three mice per dose were sacrificed at 2, 8, and 24 h after treatment. Plasma and tumor samples were collected for further analysis using high-performance liquid chromatography tandem mass spectrometry (HPLC-MS/MS; see below). Tumor samples were dried and stored at −80°C until analysis.

HPLC-MS/MS analysis of tumor and plasma samples. Quantitation of AQ4N and its metabolites, AQ4M and AQ4, from plasma and tumor samples was determined following liquid-liquid extraction in methanol containing 0.1% (v/v) acetic acid using a similar methodology that has been described previously (38). Following liquid extraction, plasma samples were added to known concentrations of the internal standard, mitoxantrone, and subjected to centrifugation at 15,000 rpm for 10 min at 4°C. The resulting supernatants were analyzed by HPLC-MS/MS as described below. Resected BxPC-3 tumor samples (~300 mg) were homogenized in cold water, added to mitoxantrone standard, and subjected to liquid-liquid extraction. Following the centrifugation of tissue homogenates, the supernatants were collected and concentrated to a final volume of 0.4 mL using a vacuum concentrator before HPLC-MS/MS analysis.

Chromatographic analysis was done using a methodology adapted from Loadman et al. (38). Briefly, AQ4N, AQ4, and AQ4M were quantitated from plasma and BxPC-3 tumor samples using a Perkin-Elmer HPLC-MS/MS system (Perkin-Elmer, Wellesley, MA). Samples were separated by HPLC using a LiChrospher RP select B 55 × 2 mm, 3 μm column protected with a 10PK HIRPB-10C guard cartridge, using a flow rate of 200 μL/min. The mass spectrometer worked in positive MS-MS mode, scanning in multiple reaction monitoring mode, using nitrogen as the collision gas. The ion transitions monitored were m/z 444>384, 412>72, 428>58, and 444>88 for AQ4N, AQ4, AQ4M, and mitoxantrone, respectively. The retention time of AQ4N, AQ4, AQ4M, and mitoxantrone was 1.7 min. Standard concentrations of AQ4N, AQ4M, and AQ4 from stock solutions were prepared in 0.1% acetic acid. Calibration curves were prepared by spiking standard concentrations in blank (drug-free) plasma from 25 to 5,000 ng/mL or blank BxPC-3 tumor homogenate from 25 to 3,000 ng/mL.

Results

***Growth inhibitory effects of AQ4N and AQ4 in human tumor cells* in vitro.** Unlike the prodrug AQ4N, the bioreduced AQ4 metabolite is a potent DNA intercalator and topoisomerase II inhibitor. We therefore compared the antiproliferative activity of AQ4 and AQ4N against a panel of human solid tumor lines under normoxia *in vitro* (Table 1). For each cell line, parallel assays were also done using appropriate standard chemotherapeutic agents for relative comparison of the cytotoxic response. Table 1 summarizes the drug concentration required to block cell growth by 50% (IC_{50}) for each tumor line treated with AQ4N, AQ4, or standard agent.

AQ4 was observed to have potent antiproliferative activity against all the solid tumor lines tested with an IC_{50} in the low micromolar range. Interestingly, AQ4 showed similar activity ranges in comparison with gemcitabine (0.4-1.6 μmol/L for AQ4; 0.02-1.7 μmol/L for gemcitabine) against the three pancreatic carcinoma tumor lines tested. Whereas gemcitabine seemed to have a greater inhibitory effect on the BxPC-3 and Mia PaCa-2 pancreatic lines, AQ4 was shown to have more potent cytotoxic effects against Panc-1 cells. In the four human

colon tumor lines tested, the activity of AQ4 was an order of magnitude lower than SN38, the activated metabolite of irinotecan and a commonly used antineoplastic agent against colorectal cancer. AQ4 showed greater effects on cell viability than paclitaxel in all three head and neck lines as well as the hepatocellular carcinoma tumor lines (0.3-3.3 μmol/L for AQ4; 2.0-19.1 μmol/L for paclitaxel). In general, AQ4 was less potent than paclitaxel against the breast, ovarian, non–small cell lung, prostate, and melanoma cell lines.

In contrast to the broad-spectrum potent activity of AQ4, AQ4N was shown to have low or unmeasurable antiproliferative activity in the majority of human tumor lines tested (Table 1). Certain tumor cell lines, including those derived from the colon, lung, and head and neck lines, seemed to be marginally sensitive to AQ4N, but their IC_{50} values (12.3-103 μmol/L) were generally orders of magnitude higher than those observed with AQ4. There was no measurable activity of AQ4N against 13 of the 21 tumor cell lines tested under the normoxic conditions used in this assay (Table 1). These data support the evidence that the bioreduced metabolite AQ4 is significantly more cytotoxic than the prodrug AQ4N against human solid tumor lines from diverse tissue types, including those derived from the pancreas.

Antitumor efficacy of AQ4N in multiple pancreatic xenograft models. Based on the potent growth-inhibitory activity of AQ4 shown in the pancreatic tumor cell lines *in vitro*, we explored the antitumor activity of AQ4N *in vivo* using human Panc-1 or BxPC-3 pancreatic xenograft models. In each case, a range of AQ4N dose schedules was evaluated to determine the optimum dosage for efficacy as a single agent. Gemcitabine, a pyrimidine antimetabolite currently used to treat advanced and metastatic pancreatic cancers, was used as a comparison for AQ4N activity in these models.

In the Panc-1 model, the end point of the study was predefined to be when tumors reached 1,200 mm^3 and treatment outcome was determined from TGD as described in Materials and Methods. As shown in Fig. 1A, AQ4N was observed to significantly inhibit the growth of Panc-1 tumors *in vivo*. AQ4N-dosed mice at 90 mg/kg q3d × 6 (given once every 3 days for a total of six times) or 120 mg/kg weekly × 8 resulted in a TGD of 20.2 days (70%; $P = 0.02$) and 27.7 days (96%; $P = 0.02$), respectively, compared with the vehicle control group. Furthermore, mice treated with AQ4N showed a significant increase in the median time to end point (49 days for AQ4N 90 mg/kg q3d × 6; 56.5 days for AQ4N 120 mg/kg weekly × 8) compared with the vehicle control-treated animals (28.8 days; Fig. 1A). In addition, both AQ4N treatment groups had significantly greater ($P = 0.02$) antitumor activity compared with the standard agent gemcitabine in this model. Mice treated with gemcitabine had a time to end point of 34.2 days, resulting in a nonsignificant TGD of 5.4 days (19%; Fig. 1A). Tumor volume measurements for each group over time following initiation of treatment are shown in Fig. 1B.

In general, AQ4N at the doses and schedules tested resulted in short-term body weight loss that was recovered following cessation of treatment (Fig. 1C). Treatment of mice with AQ4N at 90 mg/kg q3d × 6 was well tolerated as evident by a maximum body weight loss of only 4.3% observed on day 2. This was similar to gemcitabine treatment, which produced a maximum body weight loss of 5.3% on day 3. The AQ4N 120 mg/kg weekly × 8 schedule was tolerated for the initial six treatments as evident by minimal body weight loss; however, the last two treatments were less tolerated and resulted in 17.3% weight loss at day 52. Therefore, a shorter-term schedule of weekly AQ4N dosing was used in subsequent studies.

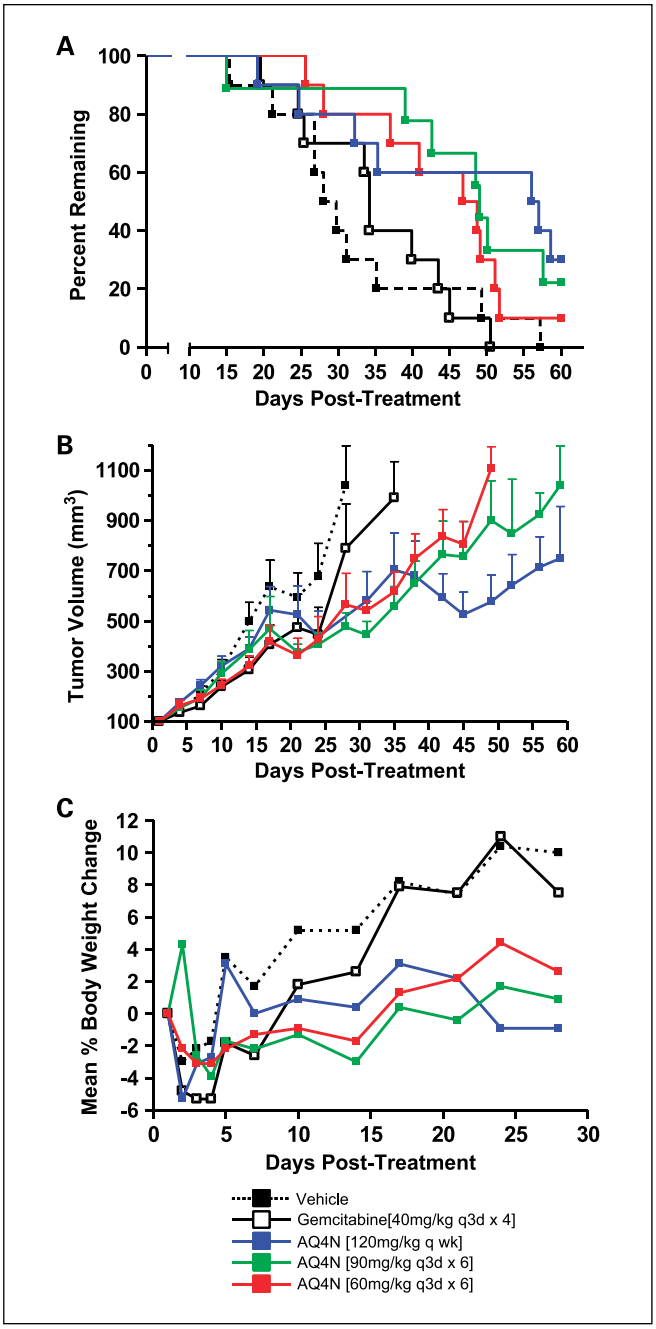

Fig. 1. AQ4N treatment significantly delays tumor growth progression in the s.c. Panc-1 pancreatic adenocarcinoma model. Human Panc-1 tumor fragments were implanted s.c. into nude mice, and AQ4N or gemcitabine treatment (at the indicated dose and schedules) was initiated when tumors reached ~100 mm^3 in size. The end point for each animal was when its tumor reached the predetermined end point size of 1,200 mm^3 or at the conclusion of the study (day 60), whichever came first. *A,* Kaplan-Meier plots summarizing the percentage of the animals remaining in the study as a function of time following initiation of treatment. *B,* effect of treatment on tumor volume over time following initiation of treatment. *C,* mean ($n = 10$) percentage body weight change of mice in each treatment group following initiation of treatment.

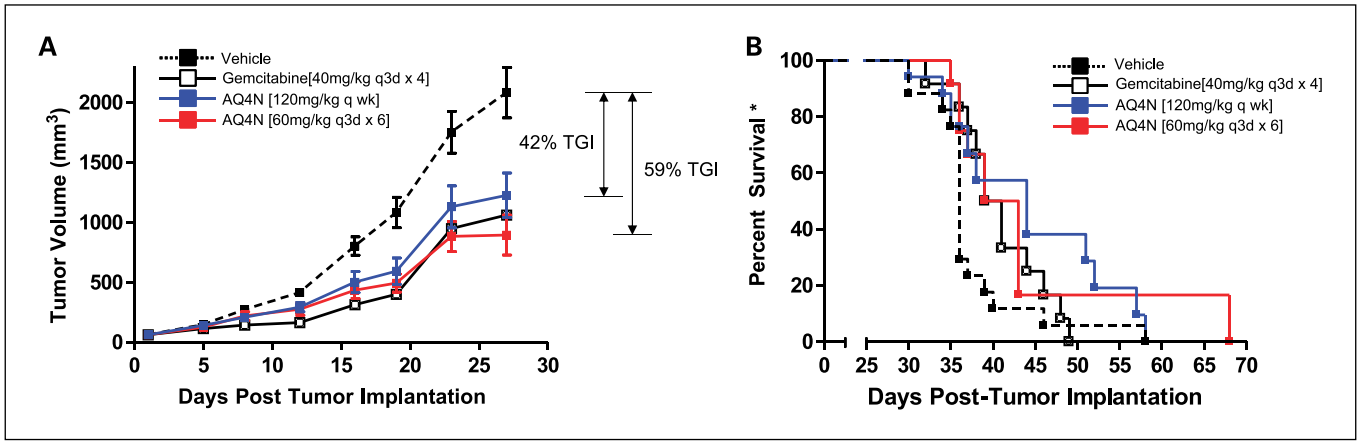

Fig. 2. Significant antitumor activity by AQ4N treatment in s.c. and orthotopic pancreatic BxPC-3 xenograft models. *A,* inhibition of s.c. implanted BxPC-3 tumors in nude mice. AQ4N or gemcitabine treatment, using the dose/schedule regimens indicated in the legend, was initiated when tumors reached approximately 60 to 80 mm^3 in size. Points, mean tumor volumes measured from treatment and control groups following tumor challenge; bars, SE. The study was terminated when tumors from the vehicle-treated group reached an average of ~2,000 mm^3 (day 27), and the %TGI was calculated as defined in the text. *B,* Kaplan-Meier plots showing prolongation of survival by AQ4N in mice bearing orthotopic implanted BxPC-3 tumors. AQ4N or gemcitabine treatment was initiated on day 14 following direct injection of tumor cells into the pancreas parenchyma. Asterisk, animals were actively sacrificed when they displayed symptoms of excessive tumor burden or treatment effects according to the criteria outlined by the Institutional Ethical Committee.

To extend our observations in other pancreatic tumor types and to explore the effects of AQ4N on metastasis, we then studied the human BxPC-3 pancreatic carcinoma model. Initially, we examined the effects of AQ4N or gemcitabine on preestablished (60-80 mm^3) BxPC-3 tumors grown s.c. using TGI as the readout. The percentage TGI, defined as the change in mean tumor volume of the treated groups/the change in mean tumor volume of the control group × 100 ($\Delta T/\Delta C$), was calculated for each group when tumors from the control group reached an average of 2,000 mm^3 (~day 27). As shown in Fig. 2A, single-agent treatment with either AQ4N or gemcitabine resulted in significant TGI in comparison with vehicle-treated groups ($P < 0.001$). Mice treated with AQ4N at 60 mg/kg q3d × 6 showed the highest TGI (58.8%) compared with the vehicle-treated control group ($P < 0.001$; Fig. 2A). In addition, weekly treatment using AQ4N at 120 mg/kg also showed significant TGI (42.4%) in a manner comparable with gemcitabine treatment (51%).

Having observed significant activity in two different s.c. models, we next investigated the effects of AQ4N in prolonging the survival of tumor-bearing mice in a more clinically relevant and highly aggressive orthotopic model of BxPC-3 pancreatic carcinoma. In this model, control mice that are surgically injected with tumor cells into the pancreas parenchyma succumb to tumor burden with a median survival time of 36 days (Fig. 2B). The same dose schedules of AQ4N (60 mg/kg q3d × 6 and 120 mg/kg q weekly × 3) that resulted in efficacy in the s.c. BxPC-3 model were also evaluated in this orthotopic model with the treatment being initiated on day 14 following tumor implantation. As shown in Fig. 2B, AQ4N treatment prolonged the survival of tumor-bearing mice in a statistically significant manner. Mice treated with AQ4N at 120 mg/kg q weekly × 3 showed a prolonged median survival of 44 days ($P = 0.05$), whereas those treated with AQ4N at 60 mg/kg q3d × 6 had a median survival time of 41 days ($P = 0.03$; Fig. 2B). Interestingly, gemcitabine treatment resulted in a similar therapeutic outcome compared with AQ4N with a median survival of 40 days ($P = 0.04$) from this highly aggressive tumor (Fig. 2B).

Effects of AQ4N treatment in reducing metastasis of orthotopic BxPC-3 tumors. Orthotopic implantation of BxPC-3 tumor cells into the pancreas of mice results in the development of metastatic lesions in multiple organs, including the liver, lymph nodes, and spleen, as detected by intravital microscopy (39). To evaluate whether AQ4N treatment had an effect on liver metastasis in this model, we did histopathologic analyses on primary liver tissue sections ($n = 5$/group) harvested on day 36 after tumor challenge (Fig. 3). As expected, gross pathologic analysis of vehicle control mice showed large invasive primary tumors at the site of the pancreas (data not shown). In addition, histologic analysis of livers from four of five control mice showed the presence of large invasive tumors; an example is seen in Fig. 3A in which a metastatic lesion of ~50% of the size of the primary tumor is seen invading the liver. In contrast, liver metastases were observed in only two of five mice following AQ4N treatment (Fig. 3B). In addition to impeding the incidence of metastatic spread, AQ4N treatment (120 mg/kg) was also observed to significantly affect the size of the invading metastatic lesion (Fig. 3A and B). The fraction of liver tissues occupied by metastatic tumor cells in comparison with the percentage of total liver tissue indicated a pronounced reduction in the size and percentage of metastatic tumors following AQ4N treatment (Fig. 3B). Although a dose response was not evaluated, the antimetastatic effects were qualitatively and quantitatively more pronounced in the 120 mg/kg AQ4N–treated group than in the 60 mg/kg AQ4N–treated group (Fig. 3A and B). Thus, in addition to having significant effects in delaying tumor growth progression and prolonging survival of tumor-bearing mice, AQ4N treatment also seems to have an effect in reducing liver metastasis emanating from orthotopically implanted BxPC-3 pancreatic tumors.

***Selective tumor targeting of the prodrug AQ4N in pancreatic xenografts* in vivo.** AQ4N is designed to be a prodrug that is inert in most tissues until it is bioactivated to a potent cytotoxin under hypoxic conditions. Although tumor hypoxia, produced by physical or chemical methods, has been shown to enhance AQ4N activity against syngeneic tumors *in vivo* (31, 40), the

selective tumor-targeting and pharmacokinetic properties of AQ4N and its metabolites in experimental human cancer models have not been studied extensively. Therefore, we evaluated the systemic and local tumor concentrations of the AQ4N prodrug and its bioreduced metabolites, AQ4M and AQ4, following treatment in BxPC-3 tumor-bearing mice using quantitative analytic procedures (HPLC-MS/MS).

As shown in Fig. 4, tumor and plasma pharmacokinetics of AQ4N, AQ4M, and AQ4 were evaluated at 2, 8, and 24 h following a single i.v. administration of AQ4N at 20, 60, 120, or 240 mg/kg. AQ4N was only detectable in plasma samples at 2 h following drug administration. Consistent with previous reports, AQ4N was observed to be rapidly eliminated from the systemic circulation, with only trace amounts

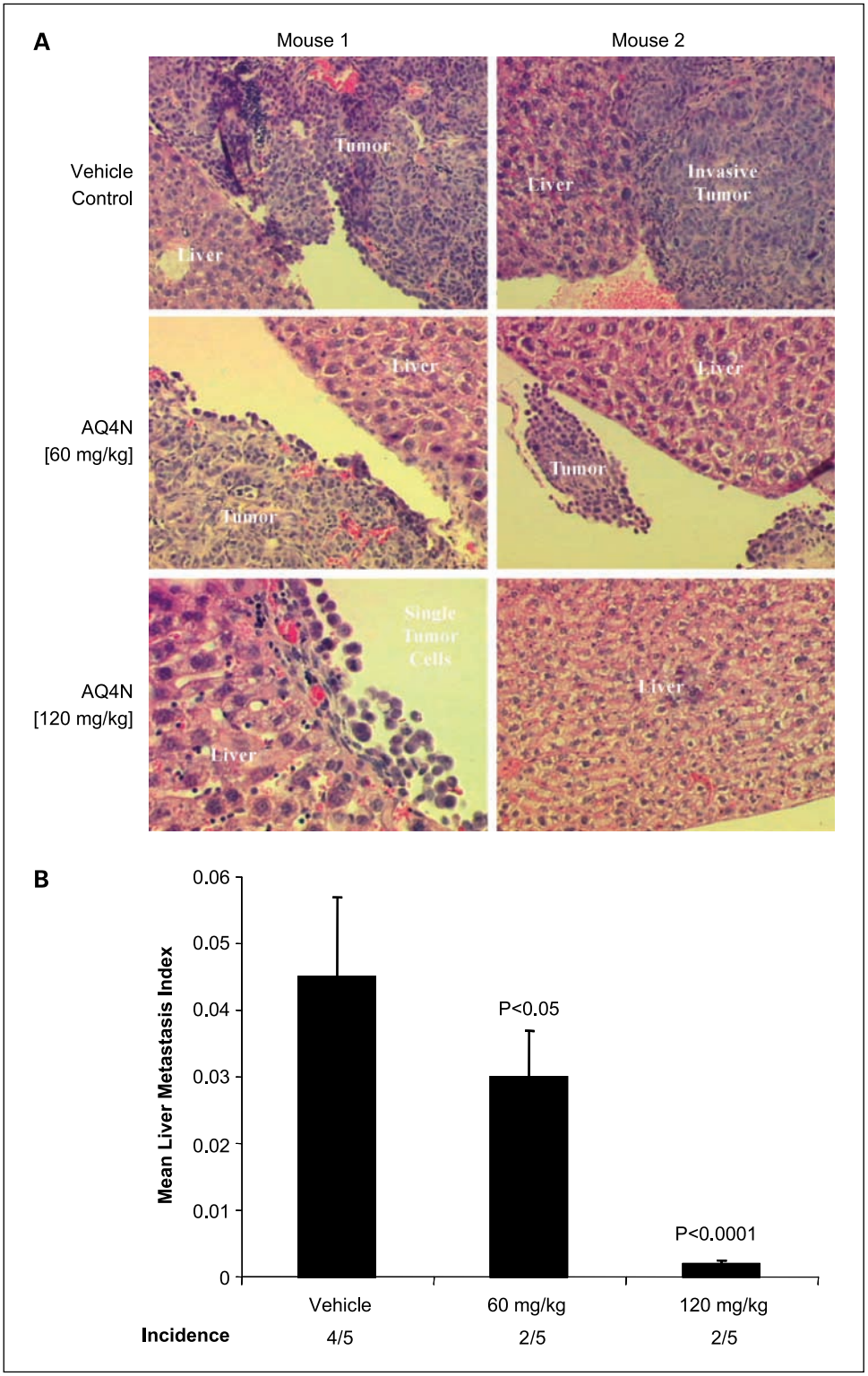

Fig. 3. Effects of AQ4N treatment on liver metastases following orthotopic BxPC-3 tumor implantation. *A,* livers were resected on day 36 after tumor challenge, paraffin embedded, and stained with H&E. Two representative H&E-stained liver sections from control-treated (*top*), 60 mg/kg AQ4N – treated (*middle*), and 120 mg/kg AQ4N – treated (*bottom*) groups. Magnification, ×100. *B,* AQ4N decreases the incidence and invasiveness of metastasis BxPC-3 lesions in the liver (n = 5/group). To compute metastasis index, five histologic sections from each liver were analyzed by microscopy and scored for the mean (±SE) percentage of area occupied by the invading BxPC-3 tumor lesion in comparison with the total liver tissue area analyzed. Evaluation of blinded samples was done by two independent operators. Statistical analysis was done using the nonparametric Mann-Whitney *U* test.

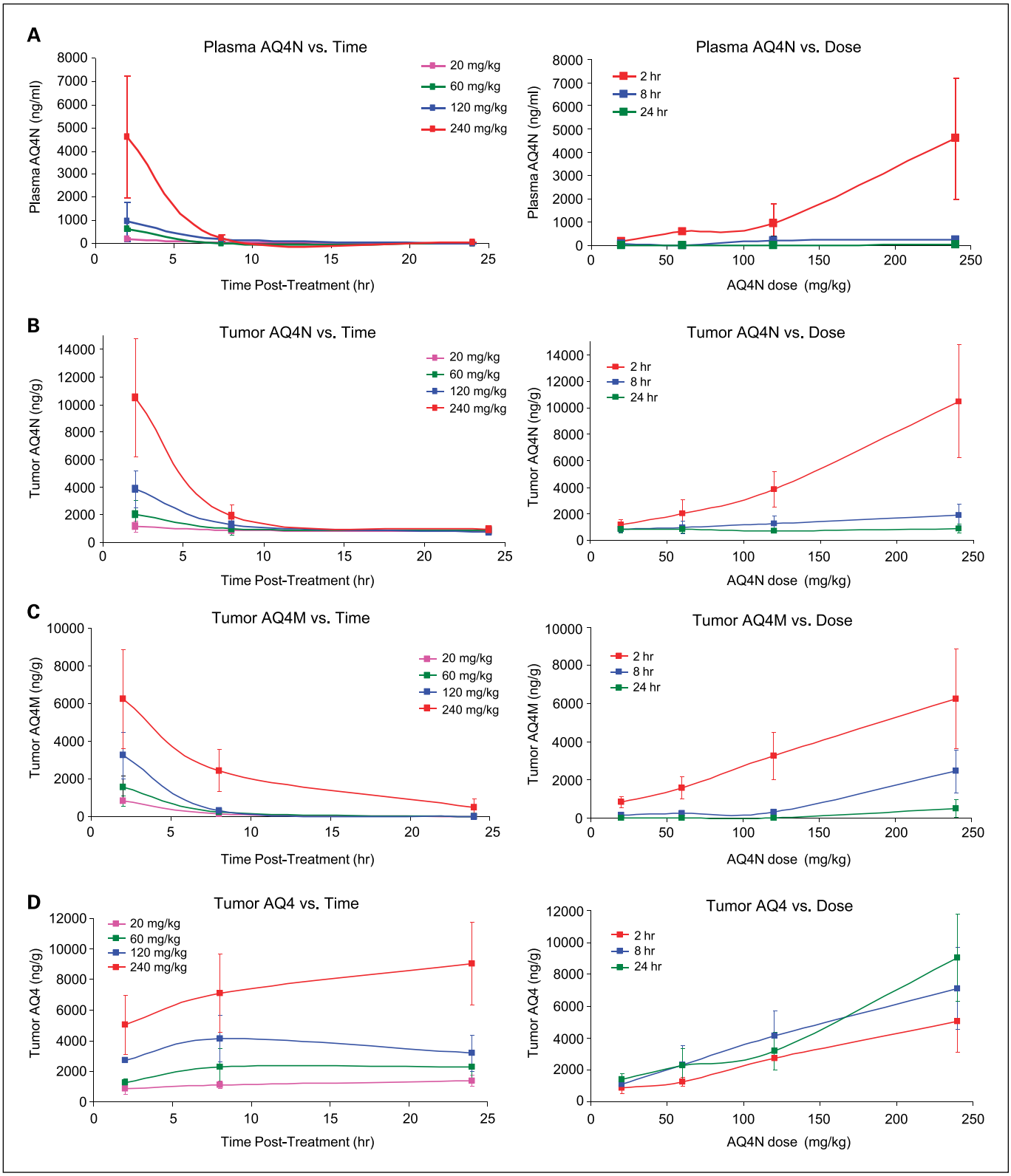

Fig. 4. Tumor and plasma pharmacokinetics of AQ4N, AQ4M, and AQ4 in BxPC-3 tumor-bearing mice. Following a single administration of 20, 60, 120, or 240 mg/kg AQ4N, primary BxPC-3 tumors or plasma samples were collected at 2, 8, and 24 h and subjected to HPLC-MS/MS for quantitative analysis. Points, mean plasma and tumor concentrations of AQ4N, AQ4M, and AQ4 plotted as a function of time after treatment (*left*) or versus treatment dose (*right*); bars, SD. *A,* plasma concentrations of AQ4N plotted versus AQ4N treatment dose or time. The bioreduced metabolites AQ4M and AQ4 were undetectable in the plasma at any of the treatment doses or time points investigated (data not shown). *B,* concentrations of AQ4N in the tumor and plotted versus treatment dose or time. *C,* concentrations of the intermediate AQ4M metabolite measured in the tumor and plotted as a function of AQ4N treatment dose or time. *D,* concentrations of the cytotoxic AQ4 metabolite measured in pancreatic tumors and plotted against the input treatment dose or time.

detectable in the plasma after 24 h at the highest dose (Fig. 4A; ref. 41). Importantly, the activated cytotoxic metabolite AQ4 was not detectable in the plasma at any dose or time point, and only trace amounts of the mono-*N*-oxide intermediate AQ4M were observed at 2 h for the 240 mg/kg dose sample (data not shown). These data indicate that AQ4N does not undergo systemic bioactivation and the prodrug is rapidly eliminated from the general circulation *in vivo*.

Consistent with its high tissue permeability, AQ4N was found at high levels in tumors only at the earliest time point (2 h) for all doses, showing rapid penetration of the prodrug into tumor tissues. Tumor levels of AQ4N were roughly linear with dose when measured at 2 h, with no evidence of saturation at the highest dose used (Fig. 4B). Concentrations of AQ4N detected in the tumor rapidly decreased over time, with little remaining at 24 h for all doses (Fig. 4B). Tumor accumulation of the mono-*N*-oxide AQ4M was approximately linear with increasing dose at 2 h following drug infusion (Fig. 4C). However, AQ4M was relatively short lived in tumors following treatment, as expected for an intermediate metabolite, and was present at minimal levels by 8 h for most doses (Fig. 4C). For the highest treatment dose of 240 mg/kg, AQ4M tumor clearance was slower as evident by the increased area under the plasma concentration versus time curve but reached substantially low levels by 24 h (Fig. 4C).

The activated cytotoxic metabolite AQ4 was found at high levels in all tumor samples at all time points, showing unambiguous localized activation of the prodrug in tumor tissues (Fig. 4D). Following treatment, AQ4 levels accumulated in the tumor in prodigious amounts (1.3-9.0 μg/g tumor tissue) and with rapid kinetics, as observed by 55% to 85% of near maximal levels after 2 h after infusion for all doses and 80% to 100% of conversion occurring by 8 h (Fig. 4D). The levels of AQ4 observed at 24 h are likely to be near maximal, as little AQ4N or AQ4M seemed available at this time point for further metabolic conversion (Fig. 4B and C). Previous studies have shown that AQ4 can be detected in tumor tissues for at least 2 weeks following a single 20 mg/kg dose of AQ4N,[3] indicating the persistence of this highly stable DNA intercalator *in vivo*. In this study, quantitative detection using HPLC-MS/MS indicates that AQ4 selectively accumulates in human BxPC-3 tumors in a nearly linear dose-dependent fashion (Fig. 4D). These data provide clear demonstration that AQ4N undergoes rapid and selective conversion into the potent antineoplastic metabolite AQ4 in pancreatic tumors *in vivo* and supports the further development of hypoxia-activated prodrugs as tumor-targeting agents.

Discussion

Pancreatic tumors display significant regions of hypoxia that are often resistant to cell killing by radiation and certain chemotherapeutics (6–10). Hypoxia-activated prodrugs, such as AQ4N, are designed to selectively target hypoxic tumor tissues while having minimal systemic toxicity. In this present study, we show for the first time that AQ4N undergoes dose-dependent and selective tumor activation *in vivo*, which results in significant inhibition of tumor growth and progression in several pancreatic xenograft models. In the aggressive BxPC-3 orthotopic model, treatment with AQ4N prolonged the median survival of tumor-bearing mice in a manner comparable with gemcitabine. Given that AQ4N may undergo metabolic activation only in hypoxic fractions, it is plausible that enhanced antitumor effects may be observed when AQ4N is combined with other agents that target oxygenated tumor regions, such as gemcitabine or radiation. In previous studies using syngeneic squamous cell carcinoma, fibrosarcoma, or mammary carcinoma models, AQ4N possessed marginal antitumor effects as a single agent but showed a >2-fold increase in activity when combined with radiation or chemotherapy (20, 31, 40, 42, 43).

In vitro, the bioreduced AQ4 metabolite was shown to inhibit the viability of multiple human pancreatic tumor lines with an apparent IC_{50} in the low micromolar range in contrast to the minimal activity of the AQ4N prodrug under normoxic conditions. The IC_{50} measured in our 3-(4,5-dimethylthiazol-2-yl)-2,5-diphenyltetrazolium bromide assays may underestimate the true cytotoxicity of AQ4 because our studies only measured cell viability indirectly at 72 h following treatment. Using the more sensitive clonogenic assay, which may be more predictive of cell killing by DNA-damaging agent conditions (31, 44), previous studies have shown that AQ4 induces cytotoxicity with submicromolar IC_{50} activity in several human tumor lines under aerobic conditions (31, 44). Nevertheless, our studies extend previous observations that the AQ4N prodrug is relatively nontoxic or displays >100-fold less toxicity compared with the bioreduced AQ4 metabolite in a broad spectrum of human tumor cell lines *in vitro*.

Hypoxia has been shown to influence metastatic disease progression in several preclinical and human studies (1, 14, 15). Prolonged tumor hypoxia increases genomic instability, selects for metastatic variants, and alters the expression of genes involved in cell adhesion, migration, and tissue remodeling (1, 11–15). Given that AQ4N is selectively activated in hypoxic cells, we postulated that treatment may influence metastatic tumor development in the malignant orthotopic BxPC-3 model. Our observations indicate that AQ4N treatment reduces the incidence and growth of micrometastatic liver tumors *in vivo*. Based on the limited number of samples and time points analyzed, it is currently unknown whether the antimetastatic effects observed are a result from the cytolysis of a subset of metastatic tumor populations at the primary site or whether AQ4N may target the growth and invasiveness of disseminated tumor cells within hypoxic sites in the liver. These results are also consistent with recent reports showing reduced metastatic tumor dissemination in murine tumor models using other hypoxia-activated cytotoxins, including tirapazamine (45).

The pharmacokinetics of AQ4N and its metabolites in plasma and tumors seem consistent with its prodrug mode of action. Linear dose-dependent accumulation of the AQ4N and its bioreduced metabolites was readily observed in tumor tissues shortly following drug infusion. The kinetics of AQ4 and AQ4M appearance support the notion that AQ4N is rapidly metabolized to AQ4 in tumors through a relatively short-lived intermediate. Although the amount of tumor AQ4 increased in a linear fashion over the range of doses tested, the therapeutic effects related to dose dependency in our tumor models were less than obvious. Our studies indicate

[3] A.S. Lalani et al., unpublished observation.

that AQ4 accumulates in BxPC-3 tumors at concentrations (3.59-20 μmol/L) that are 2- to 12.5-fold greater than the predicted IC_{50} from *in vitro* analysis. As tumor hypoxia can be heterogeneous, it is difficult to accurately assess the fraction or subset of BxPC-3 tumors that trigger AQ4N bioactivation and oncolysis. Interestingly, AQ4 was recently shown to be tumor selective and colocalize with the Glut-1 hypoxic marker in human tumor biopsies following treatment in a phase 1 pharmacodynamic study (46).

Once reduced, AQ4 is unlikely to diffuse far from its producer cell given its potent DNA-binding affinity (34). Importantly, the rapid systemic clearance of AQ4N and the absence of the metabolites in the plasma indicate that bioactivation of the prodrug does not occur in the circulation. These mass spectral data are consistent with other clinical and preclinical pharmacokinetic studies showing that systemic levels of AQ4 and AQ4M represent <2% of the input prodrug (41, 47–49). As a consequence, AQ4N would not be expected to have serious systemic toxicities *in vivo* given its primary tumor localization and limited bystander effects. Although we did not do an exhaustive analysis of other normal tissues in our pancreatic models, biodistribution studies show predominant drug localization in BxPC-3 tumors, large intestine, and spleen, which persisted for over 2 weeks following a single administration of 20 mg/kg [^{14}C-methyl]AQ4N (data not shown). Indeed, clinical exposure of AQ4N with doses as high as 750 mg/m^2 has been well tolerated with minimal systemic toxicities, including skin and urine discoloration, and fatigue (47–49). These data support the rationale for the development of bioreductive prodrugs, such as AQ4N, as a potentially safe therapy for hypoxic tumors, such as pancreatic adenocarcinomas. Further preclinical and clinical studies combining AQ4N with radiation and other chemotherapies are currently under way and may yield enhanced therapeutic effects by targeting both the oxygenated and hypoxic regions of this aggressive neoplasm.

References

1. Harris AL. Hypoxia—a key regulatory factor in tumour growth. Nat Rev Cancer 2002;2:38–47.
2. Brown JM, Wilson WR. Exploiting tumour hypoxia in cancer treatment. Nat Rev Cancer 2004;4:437–47.
3. Brown JM, Giaccia AJ. The unique physiology of solid tumors: opportunities (and problems) for cancer therapy. Cancer Res 1998;58:1408–16.
4. Williams KJ, Cowen RL, Brown LM, et al. Hypoxia in tumors: molecular targets for anti-cancer therapeutics. Adv Enzyme Regul 2004;44:93–108.
5. American Cancer Society. Cancer facts and figures 2006. Atlanta (GA): American Cancer Society; 2006.
6. Raijman I, Levin B. Exocrine tumors of the pancreas. In: Go VLM, DiMagno EP, Gardner JD, Lebenthal E, Reber HA, Scheele GA, editors. Pancreas: biology, pathology, and diseases. New York: Raven Press; 1993. p. 899–912.
7. Ranniger K, Saldino RM. Arteriographic diagnosis of pancreatic lesions. Radiology 1966;86:470–4.
8. Yassa NA, Yang J, Stein S, Johnson M, Ralls P. Gray-scale and color flow sonography of pancreatic ductal adenocarcinoma. J Clin Ultrasound 1997;25:473–80.
9. Megibow AJ. Pancreatic adenocarcinoma: designing the examination to evaluate the clinical questions. Radiology 1992;183:297–303.
10. Koong AC, Mehta VK, Le QT, et al. Pancreatic tumors show high levels of hypoxia. Int J Radiat Oncol Biol Phys 2000;48:919–22.
11. Erler JT, Bennewith KL, Nicolau M, et al. Lysyl oxidase is essential for hypoxia-induced metastasis. Nature 2006;440:1222–6.
12. Chi JT, Wang Z, Nuyten DS, et al. Gene expression programs in response to hypoxia: cell type specificity and prognostic significance in human cancers. PLoS Med 2006;3:e47.
13. Le QT, Denko NC, Giaccia AJ. Hypoxic gene expression and metastasis. Cancer Metastasis Rev 2004;23:293–310.
14. Vaupel P. The role of hypoxia-induced factors in tumor progression. Oncologist 2004;9 Suppl 5:10–7.
15. Subarsky P, Hill RP. The hypoxic tumour microenvironment and metastatic progression. Clin Exp Metastasis 2003;20:237–50.
16. Giaccia AJ, Simon MC, Johnson R. The biology of hypoxia: the role of oxygen sensing in development, normal function, and disease. Genes Dev 2004;18:2183–94.
17. Buchler P, Reber HA, Lavey RS, et al. Tumor hypoxia correlates with metastatic tumor growth of pancreatic cancer in an orthotopic murine model. J Surg Res 2004;120:295–303.
18. Hockel M, Vaupel P. Tumor hypoxia: definitions and current clinical, biologic, and molecular aspects. J Natl Cancer Inst 2001;93:266–76.
19. Shannon AM, Bouchier-Hayes DJ, Condron CM, Toomey D. Tumour hypoxia, chemotherapeutic resistance, and hypoxia-related therapies. Cancer Treat Rev 2003;29:297–307.
20. Patterson LH, McKeown SR. AQ4N: a new approach to hypoxia-activated cancer chemotherapy. Br J Cancer 2000;83:1589–93.
21. Patterson LH. Bioreductively activated antitumor N-oxides: the case of AQ4N, a unique approach to hypoxia-activated cancer chemotherapy. Drug Metab Rev 2002;34:581–92.
22. McKeown SR, Hejmadi MV, McIntyre IA, McAleer JJ, Patterson LH. AQ4N: an alkylaminoanthraquinone N-oxide showing bioreductive potential and positive interaction with radiation *in vivo*. Br J Cancer 1995;72:76–81.
23. Patterson LH. Rationale for the use of aliphatic N-oxides of cytotoxic anthraquinones as prodrug DNA binding agents: a new class of bioreductive agent. Cancer Metastasis Rev 1993;12:119–34.
24. Smith PJ, Blunt NJ, Desnoyers R, Giles Y, Patterson LH. DNA topoisomerase II-dependent cytotoxicity of alkylaminoanthraquinones and their N-oxides. Cancer Chemother Pharmacol 1997;39:455–61.
25. Raleigh SM, Wanogho E, Burke MD, McKeown SR, Patterson LH. Involvement of human cytochromes P450 (CYP) in the reductive metabolism of AQ4N, a hypoxia activated anthraquinone di-*N*-oxide prodrug. Int J Radiat Oncol Biol Phys 1998;42:763–7.
26. Raleigh SM, Wanogho E, Burke MD, Patterson LH. Rat cytochromes P450 (CYP) specifically contribute to the reductive bioactivation of AQ4N, an alkylaminoanthraquinone-di-*N*-oxide anticancer prodrug. Xenobiotica 1999;29:1115–22.
27. Patterson LH, McKeown SR, Robson T, et al. Antitumour prodrug development using cytochrome P450 (CYP) mediated activation. Anticancer Drug Des 1999;14:473–86.
28. McErlane V, Yakkundi A, McCarthy HO, et al. A cytochrome P450 2B6 meditated gene therapy strategy to enhance the effects of radiation or cyclophosphamide when combined with the bioreductive drug AQ4N. J Gene Med 2005;7:851–9.
29. Yakkundi A, McErlane V, Murray M, et al. Tumor-selective drug activation: a GDEPT approach utilizing cytochrome P450 1A1 and AQ4N. Cancer Gene Ther 2006;13:598–605.
30. McCarthy HO, Yakkundi A, McErlane V, et al. Bioreductive GDEPT using cytochrome P450 3A4 in combination with AQ4N. Cancer Gene Ther 2003;10:40–8.
31. Wilson WR, Denny WA, Pullen SM, et al. Tertiary amine N-oxides as bioreductive drugs: DACA N-oxide, nitracrine N-oxide, and AQ4N. Br J Cancer Suppl 1996;27:S43–7.
32. Rooney PH, Telfer C, McFadyen MC, Melvin WT, Murray GI. The role of cytochrome P450 in cytotoxic bioactivation: future therapeutic directions. Curr Cancer Drug Targets 2004;4:257–65.
33. Patterson LH, Murray GI. Tumour cytochrome P450 and drug activation. Curr Pharm Des 2002;8:1335–47.
34. Smith PJ, Desnoyers R, Blunt N, et al. Flow cytometric analysis and confocal imaging of anticancer alkylaminoanthraquinones and their N-oxides in intact human cells using 647-nm krypton laser excitation. Cytometry 1997;27:43–53.
35. Patterson LH, Craven MR, Fisher GR, Teesdale-Spittle P. Aliphatic amine N-oxides of DNA binding agents as bioreductive drugs. Oncol Res 1994;6:533–8.
36. Merriman RL, Hertel LW, Schultz RM, et al. Comparison of the antitumor activity of gemcitabine and ara-C in a panel of human breast, colon, lung, and pancreatic xenograft models. Invest New Drugs 1996;14:243–7.
37. Mathieu A, Remmelink M, D'Haene N, et al. Development of a chemoresistant orthotopic human non-small cell lung carcinoma model in nude mice: analyses of tumor heterogeneity in relation to the immunohistochemical levels of expression of cyclooxygenase-2, ornithine decarboxylase, lung-related resistance protein, prostaglandin E synthetase, and glutathione-*S*-transferase-α (GST)-α, GST-μ, and GST-π. Cancer 2004;101:1908–18.
38. Swaine DJ, Loadman PM, Bibby MC, Graham MA, Patterson LH. High-performance liquid chromatographic analysis of AQ4N, an alkylaminoanthraquinone N-oxide. J Chromatogr B Biomed Sci Appl 2000;742:239–45.
39. Bouvet M, Wang J, Nardin SR, et al. Real-time optical imaging of primary tumor growth and multiple metastatic events in a pancreatic cancer orthotopic model. Cancer Res 2002;62:1534–40.
40. Patterson LH, McKeown SR, Ruparelia K, et al. Enhancement of chemotherapy and radiotherapy of murine tumours by AQ4N, a bioreductively activated anti-tumour agent. Br J Cancer 2000;82:1984–90.
41. Loadman PM, Swaine DJ, Bibby MC, Welham KJ, Patterson LH. A preclinical pharmacokinetic study of the bioreductive drug AQ4N. Drug Metab Dispos 2001;29:422–6.

42. Friery OP, Gallagher R, Murray MM, et al. Enhancement of the anti-tumour effect of cyclophosphamide by the bioreductive drugs AQ4N and tirapazamine. Br J Cancer 2000;82:1469–73.

43. Gallagher R, Hughes CM, Murray MM, et al. The chemopotentiation of cisplatin by the novel bioreductive drug AQ4N. Br J Cancer 2001;85:625–9.

44. Brown JM, Attardi LD. The role of apoptosis in cancer development and treatment response. Nat Rev Cancer 2005;5:231–7.

45. Lunt SJ, Telfer BA, Fitzmaurice RJ, Stratford IJ, Williams KJ. Tirapazamine administered as a neoadjuvant to radiotherapy reduces metastatic dissemination. Clin Cancer Res 2005;11:4212–6.

46. Harris PA, Dunk CR, Albertella MR, et al. Tumour-specific activation of the hypoxic cell cytotoxin AQ4N: a phase I clinical study in solid tumors. Proc Amer Assoc Cancer Res 2006;47:571–2.

47. Benghiat A, Steward WP, Middleton M, et al. The use of pharmacokinetic and pharmacodynamic endpoints to determine dose of AQ4N given with radiotherapy (RT). J Clin Oncol 2005;23:105s.

48. Benghiat A, Steward WP, Loadman PM, et al. Phase I dose escalation study of AQ4N, a selective hypoxic cell cytotoxin, with fractionated radiotherapy (RT): first report. J Clin Oncol 2004;22:149s.

49. Sarantopoulos J, Tolcher AW, Wong A, et al. Banoxantrone (AQ4N), tissue CYP 450 targeted prodrug: the results of a phase I study using an accelerated dose escalation. J Clin Oncol 2006;24:81s.